Nuclear Mathematical and Computational Sciences: A Century in Review, A Century Anew
Gatlinburg, Tennessee, April 6-11, 2003, on CD-ROM, American Nuclear Society, LaGrange Park, IL (2003)

SPLITTING METHOD FOR SOLVING THE COARSE-MESH DISCRETIZED LOW-ORDER QUASIDIFFUSION EQUATIONS

Hikaru Hiruta and Dmitriy Y. Anistratov
Department of Nuclear Engineering
North Carolina State University
Raleigh, NC 27695-7909
hhiruta@unity.ncsu.edu; anistratov@ncsu.edu

Marvin L. Adams
Department of Nuclear Engineering
Texas A&M University
College Station, TX 77843
mladams@tamu.edu

ABSTRACT

In this paper, the development is presented of a splitting method that can efficiently solve coarse-mesh discretized low-order quasidiffusion (LOQD) equations. The LOQD problem can reproduce exactly the transport scalar flux and current. To solve the LOQD equations efficiently, a splitting method is proposed. The presented method splits the LOQD problem into two parts: (i) the D-problem that captures a significant part of transport solution in the central parts of assemblies and can be reduced to a diffusion-type equation, and (ii) the Q-problem that accounts for the complicated behavior of the transport solution near assembly boundaries. Independent coarse-mesh discretizations are applied: the D-problem equations are approximated by means of a finite-element method, whereas the Q-problem equations are discretized using a finite-volume method. Numerical results demonstrate the efficiency of the presented methodology.

Key Words: neutron transport, reactor physics calculations, splitting method

1. INTRODUCTION

The current generation of reactor physics methodology for full reactor-core calculations is based on the diffusion equation. To obtain highly accurate results using such methodology, it is necessary to address the limitations of diffusion theory. A series of significant improvements have been developed over the years by means of sophisticated methods of preparation of group cross section data, effective transport corrections at the interface of assemblies, etc [1]. An alternative approach is to create a general methodology that is based on equations that can take into account the transport effects exactly. The low-order equations of the quasidiffusion (QD) method meet this criterion [2–4]. In this paper we develop a methodology for reactor physics calculations based on the ideas of the QD method [5–8].

The QD method is an efficient approach for solving particle transport problems. The system of equations of this method consists of two parts: high-order and low-order equations. The high-order equation is the transport equation itself, and the system of the low-order equations is a set of equations for the scalar flux and current. The resulting system of equations is closed by means of linear-fractional functionals that are calculated from the solution of the high-order problem. These functionals become coefficients in the

LOQD equations. They are weakly dependent on the transport solution. It is important to note that the LOQD equations generate the exact transport solution provided the functionals are exact.

The work reported here is a part of a homogenization methodology for full-core calculations that will be used in combination with assembly-level transport calculations that utilize albedo boundary conditions, without making color-set calculations, to simulate interactions with adjacent assemblies in a reactor core [6]. Note that if the albedo boundary conditions accurately represent the presence of a different neighboring assembly, then the single-assembly transport calculation accurately reproduces the correct fine-mesh solution, and all functionals calculated from the single-assembly solution will be accurate. To generate all necessary data for the coarse-mesh LOQD equations it is necessary to calculate few-group cross sections and functionals, using the fine-mesh fine-group transport solution obtained from assembly-level calculations.

The structure of the low-order quasidiffusion (LOQD) equations is similar to the structure of the P1 and diffusion equations, which partially explains the name of the method. However, the LOQD equations reproduce exactly the scalar flux and current of the transport solution provided that the functionals are exact, because no approximation is made to derive the QD equations. Another significant difference from the P1 equations (and hence the diffusion equation) is that instead of the gradient of the scalar flux the first moment equation contains the divergence of a product of a spatially dependent tensor and the scalar flux. A consequence is that the LOQD equations do not have a self-adjoint operator, unlike the diffusion equation. This feature of the LOQD equations requires special effective methods for discretizing them and solving the resulting non-symmetric system of discretized equations. A group of efficient methods have been developed that solve this issues for a certain class of problems and type of discretizations [9–12]. However, in full-core reactor calculations, it is highly desirable to use methods that are very accurate on coarse meshes. Such discretizations of the LOQD equations give rise to a large system of algebraic equations with rather complicated structure. Thus, in this type of computational physics problem, it is necessary to develop an efficient new approach for solving the discretized equations.

A methodology that accounts for transport effects in reactor core calculations requires extra computational effort compared with solving the diffusion equation. It is highly desirable to minimize these extra costs. In this paper, we propose a splitting method that formulates two problems instead of one original LOQD problem. The first problem is a tensor diffusion equation, and hence existing advanced methods for diffusion problems can be used to solve it efficiently. The solution of the second problem is basically a transport correction to the first solution. We study ways to minimize costs for solving the second problem to optimize the solution of the overall LOQD problem.

Note that recently different research groups have begun developing methodologies for solving the transport equation for multidimensional full-core models on fine spatial grids and with fine energy groups. Here we develop a different kind of methodology accounting for transport effects, which can be directly used in existing production reactor-physics codes for full-core calculations. Our goal is to obtain an excellent approximation of the fine-mesh fine-group transport solution for approximately the cost of coarse-mesh few-group diffusion.

The reminder of the paper is organized as follows. In Sec. 2 we formulate the few-group LOQD equations. In Sec. 3 we define our splitting method for solving the LOQD equations in differential form. In Sec. 4 we present the method for calculating discontinuity factors and formulate the interface conditions for the

solution of the split problems. In Sec. 5 we present the discretization of equations of the splitting method. In Sec. 6 we demonstrate numerical solutions of test problems that simulate the interaction of MOX and uranium assemblies. We conclude with a discussion in Sec. 7.

2. THE FEW-GROUP LOW-ORDER QUASIDIFFUSION EQUATIONS

Let us consider a few group k-eigenvalue transport problem in 1D slab geometry. The LOQD equations for the group scalar flux ϕ^g and current J^g have the following form [4]:

$$\frac{d}{dx}J^g(x)+\Sigma_r^g(x)\phi^g(x)=\sum_{\substack{p=1\\p\neq g}}^{M_g}\Sigma_{s,0}^{p\to g}(x)\phi^p(x)+\frac{1}{k_{eff}}\chi^g(x)\sum_{p=1}^{M_g}\nu_f^p(x)\Sigma_f^p(x)\phi^p(x)\ , \tag{1}$$

$$\frac{d}{dx}\left(E^g(x)\phi^g(x)\right)+\Sigma_{tr}^g(x)J^g(x)=0\ , \tag{2}$$

$$a\le x\le b\ ,\quad g=1,...,M_g\ . \tag{3}$$

The boundary conditions are given by

$$J^g(a)=C_a^g\phi^g(a)\ ,\quad J^g(b)=C_b^g\phi^g(b) \tag{4}$$

in case of vacuum boudaries and

$$J^g(a)=0\ ,\quad J^g(b)=0 \tag{5}$$

in case of reflective boundaries. Note that for simplicity we consider problems with isotropic group-to-group scattering.

The functionals E^g, C_a^g, and C_b^g are calculated by means of the group angular flux $\psi^g(x,\mu)$ and defined as

$$E^g(x)=\int_{-1}^{1}\mu^2\psi^g(x,\mu)d\mu\Big/\int_{-1}^{1}\psi^g(x,\mu)d\mu\ , \tag{6}$$

$$C_a^g=\int_{-1}^{0}\mu\psi^g(a,\mu)d\mu\Big/\int_{-1}^{0}\psi^g(a,\mu)d\mu\ ,\quad C_b^g=\int_{0}^{1}\mu\psi^g(b,\mu)d\mu\Big/\int_{0}^{1}\psi^g(b,\mu)d\mu\ . \tag{7}$$

The complete system of equations of the QD method includes also the transport equation, and the resulting nonlinear problem is equivalent to the original linear transport problem. The E^g, C_a^g, and C_b^g contain all information about the transport solution. Hence, if these functionals are known exactly, then the solution of the LOQD equations is the exact transport scalar flux and current, i.e. ϕ^g and J^g. The functional E^g is spatially dependent, and this feature of E^g makes the LOQD significantly different from P1 equations, especially in multidimensional geometries. The equations (1) and (2) can be reduced to a diffusion-like group equations for the group scalar flux

$$-\frac{d}{dx}\left(\frac{1}{\Sigma_{tr}^g(x)}\frac{d}{dx}\left(E^g(x)\phi^g(x)\right)\right)+\Sigma_r^g(x)\phi^g(x)=\sum_{\substack{p=1\\p\neq g}}^{M_g}\Sigma_{s,0}^{p\to g}(x)\phi^p(x)+\frac{1}{k_{eff}}\chi^g\sum_{p=1}^{M_g}\nu_f^p\Sigma_f^p(x)\phi^p(x)\ . \tag{8}$$

The important difference from the neutron diffusion equation is that the spatially dependent E^g is a factor of the scalar flux under the second derivative. In the multidimensional case, there also exist terms with mixed derivatives of elements of the QD (Eddington) tensor [2].

3. SPLITTING METHOD FOR SOLVING THE LOQD EQUATIONS

In full-core calculations, the LOQD equations are to be solved on coarse grids each cell of which represents a part of an assembly [1]. In the new methodology the group data for each type of assembly will contain all necessary information about spatially averaged cross sections, discontinuity factors, etc., as well as quasidiffusion functionals (Eddington tensors) that are to be determined in assembly-level calculations using special albedo boundary conditions [6, 13]. Assuming that the cross sections and QD functionals are known, the iteration process for determining the k-eigenvalue and associated eigenfunction from the LOQD problem is defined as follows for a 1D problem:

$$\frac{d}{dx}J^{g[s]}+\Sigma_r^g\phi^{g[s]}=\sum_{\substack{p=1\\p\neq g}}^{M_g}\Sigma_{s,0}^{p\to g}\phi^{p[s]}+\frac{1}{k_{eff}^{[s-1]}}\chi^g\sum_{p=1}^{M_g}\nu_f^p\Sigma_f^p\phi^{p[s-1]}\ , \tag{9}$$

$$\frac{d}{dx}\left(E^g\phi^{g[s]}\right)+\Sigma_{tr}^gJ^{g[s]}=0\ , \tag{10}$$

$$J^{g[s]}(a)=C_a^g\phi^{g[s]}(a)\ ,\quad J^{g[s]}(b)=C_b^g\phi^{g[s]}(b)\ , \tag{11}$$

$$k_{eff}^{[s]}=\frac{\sum_{p=1}^{M_g}\int_a^b\nu_f^p\Sigma_f^p\phi^{p[s]}dx}{\sum_{p=1}^{M_g}\left(J^{p[s]}(b)-J^{p[s]}(a)+\int_a^b\Sigma_a^p\phi^{p[s]}dx\right)}\ , \tag{12}$$

where s is the iteration index.

To develop an efficient method for solving the LOQD equations, we split this system of equations into two problems, taking advantage of the nature of the large-scale behavior of neutron transport in fuel assemblies. On each s-iteration we solve two problems. The first problem (D-problem) is defined as

$$\frac{d}{dx}J_D^{g[s]}+\Sigma_r^g\phi_D^{g[s]}=\sum_{\substack{p=1\\p\neq g}}^{M_g}\Sigma_{s,0}^{p\to g}\phi_D^{p[s]}+\frac{1}{k_{eff}^{[s-1]}}\chi^g\sum_{p=1}^{M_g}\nu_f^p\Sigma_f^p\phi^{p[s-1]}\ , \tag{13}$$

$$\widehat{E}^g\frac{d}{dx}\phi_D^{g[s]}+\Sigma_{tr}^gJ_D^{g[s]}=0\ , \tag{14}$$

$$J_D^{g[s]}(a)=C_a^g\phi_D^{g[s]}(a)\ ,\quad J_D^{g[s]}(b)=C_b^g\phi_D^{g[s]}(b)\ , \tag{15}$$

Here $\widehat{E}^g(x)$ is a piece-wise constant function on a set of coarse-mesh cells. The method for choosing the values of $\widehat{E}^g$ in each cell is discussed below.

The second problem (Q-problem) is given by

$$\frac{d}{dx}J_Q^{g[s]}+\Sigma_r^g\phi_Q^{g[s]}=\sum_{\substack{p=1\\p\neq g}}^{M_g}\Sigma_{s,0}^{p\to g}\phi_Q^{p[s]}\ , \tag{16}$$

$$\frac{d}{dx}\left(E^g\phi_Q^{g[s]}\right)+\Sigma_{tr}^gJ_Q^{g[s]}=\widehat{E}^g\frac{d}{dx}\phi_D^{g[s]}-\frac{d}{dx}\left(E^g\phi_D^{g[s]}\right)\ , \tag{17}$$

$$J_Q^{g[s]}(a)=C_a^g\phi_Q^{g[s]}(a)\ ,\quad J_Q^{g[s]}(b)=C_b^g\phi_Q^{g[s]}(b)\ . \tag{18}$$

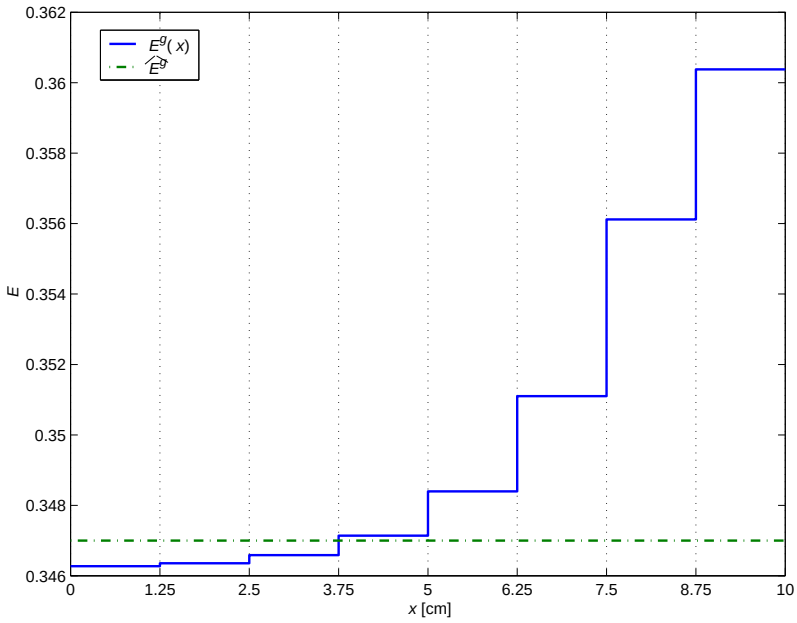

Figure 1. Pin-cell average values of E^g in thermal group in a model assembly.

The group scalar flux and current are the sums of the corresponding solutions of the above two problems

$$\phi^{g[s]} = \phi_D^{g[s]} + \phi_Q^{g[s]} \ , \quad J^{g[s]} = J_D^{g[s]} + J_Q^{g[s]} \ . \tag{19}$$

The equations of the resulting D-problems are similar to P1 equations, and, thus, they can be reduced to a diffusion equation. The differential operator of the D-problem is self-adjoint. All these features of the D-problem enable one to use high-order approximations and efficient iterative methods that were previously developed for the diffusion equation. Note that if the cross sections in Eqs. (13)-(15) are constant in each cell, it is possible to obtain solutions in analytic form and use them in expansion of ϕ_D^g for the discretization of these equations [14]. This can significantly increase accuracy of the numerical solution of the overall problem. The Q-problem equations have properties that are similar to those of the original LOQD equations described above. The extension of this splitting method to multidimensional geometries is straightforward.

Figure 1 shows pin-cell average values of the functional E^g in the thermal group across a model assembly. The left boundary corresponds to the center of an assembly, whereas the right boundary is the interface with an unlike assembly. This figure demonstrates a typical shape of E^g within assemblies. Note that the large-scale behavior of the functional E^g is such that it is almost flat in the central part (interior) of an assembly and changes in vicinity of assembly boundaries, having a form of “bath-tub” function across the assembly. Hence, if we choose $\widehat{E}^g$ as an average value of $E^g(x)$ over the interior of the assembly (in this particular case over $0 \leq x \leq 5$), then the terms in the right-hand side of Eq. (17) will be small in the central part of assemblies. Thus, in our methodology we define $\widehat{E}^g$ in the following way

$$\widehat{E}^g = \frac{\int\limits_{interior} E^g(x)\phi^{g,fm}(x)dx}{\int\limits_{interior} \phi^{g,fm}(x)dx} \ , \tag{20}$$

where $\phi^{g,fm}$ is the fine-mesh scalar flux obtained from assembly-level transport calculations.

The solution ϕ_D of the D-problem (13)-(15) captures a significant part of the transport solution in the central parts of assemblies. The solution ϕ_Q of the Q-problem (16)-(18) accounts for the complicated behavior of the transport solution near interfaces between unlike assemblies. Note that if in the D-problem we neglect ϕ_Q, then in Eq. (13) $\phi = \phi_D$. Thus, the system of equations for ϕ_D is similar to P1 equations with a modified diffusion coefficient

$$D^g = \frac{\widehat{E}^g}{\Sigma_{tr}^g} \, . \tag{21}$$

Hereafter we refer to such problem for ϕ_D as modified diffusion.

4. CALCULATION OF DISCONTINUITY FACTORS AND INTERFACE CONDITIONS FOR GLOBAL CALCULATIONS

4.1. Discontinuity Factors

The single-assembly calculations with albedo boundary conditions generate the fine-mesh fine-group transport solution, $\phi^{g,fm}$, $J^{g,fm}$, k_{eff}^{fm}, which is used to compute necessary assembly-averaged cross sections and functionals [6]. Another component of the group data is a set of discontinuity factors. To calculate them for the LOQD equations (1) and (2), one needs to solve these equations for an assembly with boundary conditions defined by the known fine-mesh currents, i.e.

$$J^g|_{x=x_\gamma} = J^{g,fm}|_{x=x_\gamma} \quad x_\gamma \in \partial\Gamma \, . \tag{22}$$

where $\partial\Gamma$ is the boundary of an assembly. In case of the splitting method, we need to formulate specific boundary conditions for both D- and Q-problems that will meet the following condition:

$$(J_D^g + J_Q^g)|_{x=x_\gamma} = J^{g,fm}|_{x=x_\gamma} \quad x_\gamma \in \partial\Gamma \, . \tag{23}$$

The choice of boundary conditions for each of two problems is not unique. We have chosen to impose the following boundary conditions:

$$J_D^g|_{x=x_\gamma} = J^{g,fm}|_{x=x_\gamma}, \quad J_Q^g|_{x=x_\gamma} = 0 \quad x_\gamma \in \partial\Gamma \, , \tag{24}$$

which is similar to the way the fission term was split between two problems. Note that there is no a priori information on the ratio between J_D^g and J_Q^g that could be used to split the known boundary current between the two.

Finally, to determine the discontinuity factors, we calculate auxiliary functions $\phi_D^{*,g}$ and $\phi_Q^{*,g}$ as the solution of the differential problem defined as:

$$\frac{d}{dx} J_D^{*,g} + \Sigma_r^g \phi_D^{*,g} = \sum_{\substack{p=1 \\ p\neq g}}^{M_g} \Sigma_{s,0}^{p\to g} \phi_D^{*,p} + \frac{1}{k_{eff}^{fm}} \chi^g \sum_{p=1}^{M_g} \nu_f^p \Sigma_f^p \phi^{p,fm} \, , \tag{25}$$

$$\widehat{E}^g \frac{d}{dx} \phi_D^{*,g} + \Sigma_{tr}^g J_D^{*,g} = 0 \, , \tag{26}$$

$$J_D^{*,g}|_{x=x_\gamma} = J^{g,fm}|_{x=x_\gamma} \, , \tag{27}$$

$$\frac{d}{dx} J_Q^{*,g} + \Sigma_r^g \phi_Q^{*,g} = \sum_{\substack{p=1 \\ p\neq g}}^{M_g} \Sigma_{s,0}^{p\to g} \phi_Q^{*,p} \, , \tag{28}$$

$$\frac{d}{dx}\left(E^g\phi_Q^{*,g}\right)+\Sigma_{tr}^g J_Q^{*,g}=\widehat{E}^g\frac{d}{dx}\phi_D^{*,g}-\frac{d}{dx}\left(E^g\phi_D^{*,g}\right)\ , \tag{29}$$

$$J_Q^{*,g}\Big|_{x=x_\gamma}=0\ , \tag{30}$$

$$\phi^{*,g}=\phi_D^{*,g}+\phi_Q^{*,g}\ . \tag{31}$$

As a result, we obtain the auxiliary function $\phi^{*,g}$ that reproduces the fine-mesh eigenvalue, assembly-averaged scalar flux and current at boundaries of an assembly. The discontinuity factors G^g at assembly boundaries are defined as:

$$G^g=\frac{\phi^{g,fm}}{\phi^{*,g}}\Big|_{x=x_\gamma}\qquad x_\gamma\in\partial\Gamma\ . \tag{32}$$

Note that the final algorithm of calculation of the auxiliary function is defined for equations (25)-(31) in discretized form, and only zeroth moment of the fission source term is defined by means of the fine-mesh transport solution. Other algorithms can be formulated as well. They would generate auxiliary functions $\phi^{*,g}$ with different features.

4.2. Interface Conditions

In global calculations on a coarse mesh, it is necessary to impose interface conditions at each coarse-cell edge, $x=x_{edge}^{cell}$,

$$J^g|_{x=x_{edge}^{cell}-0}=J^g|_{x=x_{edge}^{cell}+0}\ , \tag{33}$$

$$[G^g\phi^g]|_{x=x_{edge}^{cell}-0}=[G^g\phi^g]|_{x=x_{edge}^{cell}+0} \tag{34}$$

that express current continuity and discontinuity of the coarse-mesh scalar flux at the interface between coarse cells. For the equations of splitting method, we specify interface conditions for D- and Q-components of the solution. Based on conditions (33) and (34), we define the interface conditions for D- and Q-problems as

$$J_D^g|_{x=x_{edge}^{cell}-0}=J_D^g|_{x=x_{edge}^{cell}+0}\ ,\quad J_Q^g|_{x=x_{edge}^{cell}}=0\ , \tag{35}$$

$$\left[G^g(\phi_D^g+\phi_Q^g)\right]\Big|_{x=x_{edge}^{cell}-0}=\left[G^g(\phi_D^g+\phi_Q^g)\right]\Big|_{x=x_{edge}^{cell}+0}\ . \tag{36}$$

Note that these interface conditions give rise to independent Q-problems in each coarse-cell, which are very inexpensive to solve.

5. INDEPENDENT COARSE-MESH DISCRETIZATION OF THE LOQD EQUATIONS IN SPLIT FORM

We use different methods to approximate equations of D- and Q-problems, i.e. independent discretization. The solution of the D-problem accounts for the major part of the transport solution, and we use high-order accuracy methods to discretize its equations. The structure of these equations gives us an opportunity to use sophisticated discretization methods developed for the diffusion equation. To solve the equations of the Q-problem, we apply a discretization method with second-order accuracy. Here we consider this approach in 1D case to study basic features of the proposed methodology.

5.1. Discretization of the D-Problem Equations

Let us define the coarse mesh $\{x_{j-1/2},\ j=1,...,N_j+1,\ x_{1/2}=a,\ x_{N_j+1/2}=b\}$. The D-problem equations (13)-(15) are discretized utilizing a high-order finite-element method based on the following expansion of the scalar flux $\Phi^g_{D,j}(x)$ in each jth coarse cell ($x_{j-1/2}\le x\le x_{j+1/2}$):

$$\Phi^g_{D,j}(x)=\sum_{l=0}^{2}(2l+1)\varphi^{(l),g}_{D,j}P_l(\zeta_j(x))+\varphi^{(3),g}_{D,j}\sinh(\varkappa^g_{D,j}(x-x_j))+\varphi^{(4),g}_{D,j}\cosh(\varkappa^g_{D,j}(x-x_j))\,, \quad (37)$$

where P_l are Legendre polynomials,

$$\zeta_j(x)=\frac{2(x-x_j)}{H_j},\quad H_j=x_{j+1/2}-x_{j-1/2},\quad x_j=0.5(x_{j+1/2}+x_{j-1/2}),\quad 1\le j\le N_j\,, \quad (38)$$

$$\varkappa^g_{D,j}=\sqrt{\frac{\langle\Sigma_r\rangle^g_j\langle\Sigma_{tr}\rangle^g_j}{\widehat{E}^g_j}}\,. \quad (39)$$

Hereafter we use brackets $\langle\bullet\rangle$ to denote the coarse-mesh averaged cross sections generated by means of fine-mesh scalar flux $\phi^{g,fm}$ obtained from assembly-level transport calculations.

To discretize the D-problem equations, we integrate the balance equation (13) over the jth coarse cell with Legendre polynomials as weight functions and approximate Eq. (14) at coarse-cell edges using the information from pin-cells next to the boundaries of the given coarse cell [14]. Then, we formulate a set of discrete equations for Legendre moments of the coarse-cell scalar flux

$$\Phi^{(l),g}_{D,j}=\frac{1}{H_j}\int\limits_{x_{j-1/2}}^{x_{j+1/2}}P_l(\zeta_j(x))\Phi^g_{D,j}(x)dx\,,\quad l=0,1,2\,, \quad (40)$$

cell-edge scalar fluxes, $\Phi^g_{D,j}(x_{j\pm1/2})$, and currents, $J^g_{D,j+1/2}\overset{\text{def}}{=}J^g_D(x_{j+1/2})$. The discretization scheme for the D-problem equations is defined as

$$J^g_{D,j+1/2}-J^g_{D,j-1/2}+\langle\Sigma_r\rangle^g_jH_j\Phi^{(0),g}_{D,j}=H_j\sum_{\substack{p=1\\p\neq g}}^{M_g}\langle\Sigma_{s,0}\rangle^{p\to g}_j\Phi^{(0),p}_{D,j}+\frac{1}{k_{eff}}H_j\sum_{p=1}^{M_g}\langle\chi\nu\Sigma_f\rangle^{p,g}_j\Phi^{(0),p}_j\,, \quad (41)$$

$$J^g_{D,j+1/2}+J^g_{D,j-1/2}+\frac{2\widehat{E}^g_j}{\langle\Sigma_{tr}\rangle^g_jH_j}\left(\Phi^g_{D,j}(x_{j+1/2})-\Phi^g_{D,j}(x_{j-1/2})\right)+\langle\Sigma_r\rangle^g_jH_j\Phi^{(1),g}_{D,j}= \quad (42)$$

$$H_j\sum_{\substack{p=1\\p\neq g}}^{M_g}\langle\Sigma_{s,0}\rangle^{p\to g}_j\Phi^{(1),p}_{D,j}+\frac{1}{k_{eff}}H_j\sum_{p=1}^{M_g}\langle\chi\nu\Sigma_f\rangle^{p,g}_j\Phi^{(1),p}_j\,,$$

$$J^g_{D,j+1/2}-J^g_{D,j-1/2}+\frac{6\widehat{E}^g_j}{\langle\Sigma_{tr}\rangle^g_jH_j}\left(\Phi^g_{D,j}(x_{j+1/2})+\Phi^g_{D,j}(x_{j-1/2})-2\Phi^{(0),g}_{D,j}\right)+\langle\Sigma_r\rangle^g_jH_j\Phi^{(2),g}_{D,j}= \quad (43)$$

$$H_j\sum_{\substack{p=1\\p\neq g}}^{M_g}\langle\Sigma_{s,0}\rangle^{p\to g}_j\Phi^{(2),p}_{D,j}+\frac{1}{k_{eff}}H_j\sum_{p=1}^{M_g}\langle\chi\nu\Sigma_f\rangle^{p,g}_j\Phi^{(2),p}_j\,,$$

$$\widehat{E}_j^g \left. \frac{d\Phi_{D,j}^g}{dx} \right|_{x=x_{j-1/2}} + \{\Sigma_{tr}\}_j^{g,-} J_{D,j-1/2}^g = 0\,, \tag{44}$$

$$\widehat{E}_j^g \left. \frac{d\Phi_{D,j}^g}{dx} \right|_{x=x_{j+1/2}} + \{\Sigma_{tr}\}_j^{g,+} J_{D,j+1/2}^g = 0\,, \tag{45}$$

$$j = 1, ..., N_j\,,$$

$$G_j^{g,+}\left(\Phi_{D,j}^g(x_{j+1/2}) + \Phi_{Q,j}^g(x_{j+1/2})\right) = G_{j+1}^{g,-}\left(\Phi_{D,j+1}^g(x_{j+1/2}) + \Phi_{Q,j+1}^g(x_{j+1/2})\right)\,, \tag{46}$$

$$j = 1, ..., N_j - 1\,,$$

$$J_{D,1/2}^g = C_a^g G_1^{g,-}\left(\Phi_{D,1}^g(x_{1/2}) + \Phi_{Q,1}^g(x_{1/2})\right)\,, \tag{47}$$

$$J_{D,N_j+1/2}^g = C_b^g G_{N_j}^{g,+}\left(\Phi_{D,N_j}^g(x_{N_j+1/2}) + \Phi_{Q,N_j}^g(x_{N_j+1/2})\right)\,, \tag{48}$$

where

$$\Phi_j^{(l),g} \stackrel{\text{def}}{=} \frac{1}{H_j} \int\limits_{x_{j-1/2}}^{x_{j+1/2}} P_l(\zeta_j(x))\phi^g(x)dx\,. \tag{49}$$

Here $G_j^{g,\pm}$ are the right and left discontinuity factors, respectively, $\{\Sigma_{tr}\}_j^{g,\pm}$ are cross sections averaged over boundary pin-cell next to the right and left edges of jth coarse cell, correspondingly. Substituting the expansion (37) into Eqs. (41)-(48), we get the equations for the expansion coefficients $\varphi_{D,j}^{(l),g}$ (l=0,...,4) and cell-edge currents $J_{D,j-1/2}^g$.

5.2. Discretization of the Q-Problem Equations

Assume that a coarse-mesh cell represents half of an assembly. Such meshes are in common practice. To discretize the Q-problem equations, we divide each jth coarse cell into two subcells that are defined by $\tilde{x}_{j,i}$, i=1,2,3, where $\tilde{x}_{j,1} = x_{j-1/2}$ and $\tilde{x}_{j,3} = x_{j+1/2}$. The width of subcells is determined by the large-scale behavior of the functional E^g within a given coarse-mesh cell. A second-order finite-volume method described in previous publications [15] is used to approximate the equations (16)-(18). Note that if a coarse-mesh cell corresponds to a whole assembly, then four subcells are needed.

If we integrate Eq. (16) over each subcell and Eq. (17) over half-subcells, then make simple approximations [15], we obtain a system of discrete equations for subcell-edge currents $J_{Q,j,i}^g \stackrel{\text{def}}{=} J_Q^g(\tilde{x}_{j,i})$, coarse-cell edge scalar fluxes $\Phi_{Q,j}^{g,\pm} \stackrel{\text{def}}{=} \phi_Q^g(x_{j\pm1/2})$, and subcell-average scalar fluxes

$$\bar{\Phi}_{Q,j,i}^g \stackrel{\text{def}}{=} \frac{1}{h_{j,i}} \int_{\tilde{x}_{j,i}}^{\tilde{x}_{j,i+1}} \phi_Q^g(x)dx\,, \tag{50}$$

where $h_{j,i} = \tilde{x}_{j,i+1} - \tilde{x}_{j,i}$. The equations are:

$$J_{Q,j,i+1}^g - J_{Q,j,i}^g + \langle\Sigma_r\rangle_j^g h_{j,i}\bar{\Phi}_{Q,j,i}^g = h_{j,i}\sum_{\substack{p=1\\p\neq g}}^{M_g}\langle\Sigma_{s,0}\rangle_j^{p\to g}\bar{\Phi}_{Q,j,i}^p\,, \quad i = 1, 2\,, \tag{51}$$

$$\bar{E}^g_{j,1}\bar{\Phi}^g_{Q,j,1} - \{E\}^{g,-}_j \Phi^{g,-}_{Q,j} + \frac{1}{2}\{\Sigma_{tr}\}^{g,-}_j h_{j,1} J^g_{Q,j,1} = \left(\widehat{E}^g_j - \bar{E}^g_{j,1}\right)\bar{\Phi}^g_{D,j,1} - \left(\widehat{E}^g_j - \{E\}^{g,-}_j\right)\Phi^g_{D,j}(x_{j-1/2})\,, \tag{52}$$

$$\bar{E}^g_{j,2}\bar{\Phi}^g_{Q,j,2} - \bar{E}^g_{j,1}\bar{\Phi}^g_{Q,j,1} + \frac{1}{2}\langle\Sigma_{tr}\rangle^g_j H_j J^g_{Q,j,2} = \left(\widehat{E}^g_j - \bar{E}^g_{j,2}\right)\bar{\Phi}^g_{D,j,2} - \left(\widehat{E}^g_j - \bar{E}^g_{j,1}\right)\bar{\Phi}^g_{D,j,1}\,, \tag{53}$$

$$\{E\}^{g,+}_j \Phi^{g,+}_{Q,j} - \bar{E}^g_{j,2}\bar{\Phi}^g_{Q,j,2} + \frac{1}{2}\{\Sigma_{tr}\}^{g,+}_j h_{j,2} J^g_{Q,j,3} = \left(\widehat{E}^g_j - \{E\}^{g,+}_j\right)\Phi^g_{D,j}(x_{j+1/2}) - \left(\widehat{E}^g_j - \bar{E}^g_{j,2}\right)\bar{\Phi}^g_{D,j,2}\,, \tag{54}$$

$$j = 1, ..., N_j\,,$$

$$J^g_{Q,j,3} = 0\,, \tag{55}$$

$$J^g_{Q,j+1,1} = J^g_{Q,j,3}\,, \tag{56}$$

$$j = 1, ..., N_j - 1\,,$$

$$J^g_{Q,1,1} = 0\,, \quad J^g_{Q,N_j,3} = 0\,, \tag{57}$$

where

$$\bar{\Phi}^g_{D,j,i} \stackrel{\text{def}}{=} \frac{1}{h_{j,i}}\int_{\tilde{x}_{j,i}}^{\tilde{x}_{j,i+1}} \phi^g_D(x)dx \tag{58}$$

and $\bar{E}^g_{j,i}$ is the value of functional E^g averaged by means of the fine-mesh scalar flux over the given subcell region. $\{E\}^{g,\pm}_j$ are values of the QD functional averaged over the boundary pin-cell next to the right and left edges of jth coarse cell, respectively. The quantities $\bar{\Phi}^g_{D,j,i}$ defined by Eq. (58) are calculated from the solution of the D-problem, i.e. in the following way:

$$\bar{\Phi}^g_{D,j,i} = \frac{1}{h_{j,i}}\int_{\tilde{x}_{j,i}}^{\tilde{x}_{j,i+1}} \Phi^g_{D,j}(x)dx \tag{59}$$

In order to solve the coupled systems of D- and Q- problems, we need to calculate the Legendre spatial moments of ϕ^g_Q

$$\Phi^{(l),g}_{Q,j} \stackrel{\text{def}}{=} \frac{1}{H_j}\int_{x_{j-1/2}}^{x_{j+1/2}} P_l(\zeta_j(x))\phi^g_Q(x)dx\,, \quad l = 0, 1, 2\,, \tag{60}$$

using the solution of the above discrete equations (51)-(57). The zeroth moment is computed as

$$\Phi^{(0),g}_{Q,j} = \frac{1}{H_j}\sum_{i=1}^{2} \bar{\Phi}^g_{Q,j,i} h_{i,j}\,. \tag{61}$$

The other two spatial moments are calculated, using approximation of ϕ^g_Q in jth coarse cell by means of a third-order polynomial interpolation function that fits coarse-cell edge values $\Phi^{g,\pm}_{Q,j}$ and two subcell-average values $\bar{\Phi}^g_{Q,j,i}$. As a result for $\Phi^{(l),g}_j$ (Eq. (49)) we get

$$\Phi^{(l),g}_j = \Phi^{(l),g}_{D,j} + \Phi^{(l),g}_{Q,j} \quad l = 0, 1, 2\,. \tag{62}$$

The position of interface between subcells (i.e. $\tilde{x}_{j,2}$) is chosen such that one subcell covers the region where E^g is almost flat and another subcell corresponds to the area where E^g changes significantly near the interface with neighboring assembly. For example, in the case that is shown in Figure 1, it is reasonable to use $\tilde{x}_{j,2} = 5$.

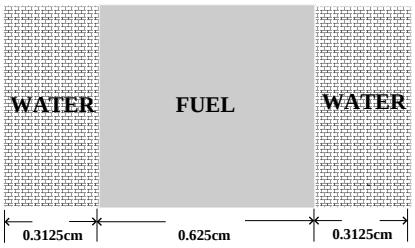

Figure 2. Pin-cell design.

6. NUMERICAL RESULTS

In this section, we present the numerical results to demonstrate the performance of the proposed splitting method. We consider two test problems (Test A and B) for 1D slab geometry with two energy groups. They consist of MOX and uranium half-assemblies next to each other with reflective boundary conditions [8, 16]. The half-assembly width is 10 cm. The MOX assembly is located on the left of UO_2 assembly. Each half-assembly contains 8 fuel pin cells of the same type. The design of a fuel pin is shown in Figure 2. The cross sections for each test problem are listed in Tables I and II. The fine-mesh solutions are calculated by the QD method using the second order finite-volume scheme for the LOQD equations and step characteristic method for the transport equation [15]. The fine mesh is uniform and consists of 128 equal cells (8 per pin cell). The angular mesh has 10 intervals. The multiplication factors in Tests A and B equal 1.5. The coarse mesh consists of one cell per half-assembly, i.e. $N_j = 2$. We recall that to solve the Q-problem, we define two subcells per coarse cell. Table III presents the values of $\widehat{E}^g$ used in these test problems. These values are generated by averaging fine-mesh E^g with fine-mesh scalar flux over the subcells adjacent to reflective boundaries. These subcells represent the interior assembly regions, where the functional E^g varies weakly. In our calculations, the subcells adjacent to the interface between assemblies are 3 pin cells wide, and the subcells next to reflective boundaries are 5 pin cells wide.

To evaluate the accuracy of the splitting method with independent discretization of equations, we use the numerical results obtained by means of a high-order finite-element (HOFE) method developed for solving LOQD equations [14]. We also apply the proposed splitting method (Eqs. (13)-(19)) to the discrete equations of the HOFE method and derived corresponding discretization of equations for D- and Q-problems, where the equations of both problems are approximated by the HOFE method. Note that this can be considered as consistent way of discretizing the equations of the splitting method. This enables us to analyze the accuracy of each part of solution, ϕ_D and ϕ_Q, by the proposed independent discretization.

Figures 3, 4, 9, and 10 show the group scalar fluxes for Tests A and B obtained by the proposed splitting method with independent discretization and the results of the HOFE method for the LOQD equations. The x-axis gridlines correspond to pin-cell boundaries. These figures also demonstrate the solution of the diffusion equation ($E^g(x) = \frac{1}{3}$) calculated by means of the HOFE method. We note that in fast group the diffusion solution has significantly different spatial shape and, thus, its behavior is qualitatively different compared with the coarse-mesh transport solution that is represented by solution of the LOQD equations. The quantitative difference between transport and diffusion solutions in thermal group is not seen because of the scale. We explicitly demonstrate the relative difference between the transport and diffusion solutions on Figures 5, 6, 11, and 12. These graphs show that the largest relative errors in diffusion solution are the following: (a) $4{\cdot}10^{-3}$ in fast group and $2{\cdot}10^{-2}$ in thermal group for Test A, (b) $7{\cdot}10^{-3}$ in both fast and

Table I. Cross Sections for Test A.

Cross Sections	Σ_t^1	$\Sigma_{s,0}^{1\to1}$	$\Sigma_{s,0}^{1\to2}$	Σ_f^1	ν_f^1	Σ_t^2	$\Sigma_{s,0}^{2\to2}$	$\Sigma_{s,0}^{2\to1}$	Σ_f^2	ν_f^2
MOX fuel	0.2	0.2	0	0	0	0.6	0	0	0.6	1.5
Uranium fuel	0.2	0.2	0	0	0	0.2	0	0	0.2	1.5
Water	0.2	0.17	0.03	0	0	1.1	1.1	0	0	0

Table II. Cross Sections for Test B.

Cross Sections	Σ_t^1	$\Sigma_{s,0}^{1\to1}$	$\Sigma_{s,0}^{1\to2}$	Σ_f^1	ν_f^1	Σ_t^2	$\Sigma_{s,0}^{2\to2}$	$\Sigma_{s,0}^{2\to1}$	Σ_f^2	ν_f^2
MOX fuel	0.2	0.185	0.015	0	0	1.2	0.9	0	0.3	1.5
Uranium fuel	0.2	0.185	0.015	0	0	1.0	0.9	0	0.1	1.5
Water	0.2	0.17	0.03	0	0	1.1	1.1	0	0	0

Table III. $\widehat{E}^g$ for Test A and B.

g	Region	Test A	Test B
1	MOX	0.3330	0.3327
1	UO_2	0.3340	0.3345
2	MOX	0.3470	0.3332
2	UO_2	0.3522	0.3331

thermal groups for Test B.

The scalar fluxes of the proposed splitting method have very good agreement with those of the HOFE method. In both test problems, the maximum relative differences between the scalar fluxes obtained by the splitting and the HOFE methods are (i) Test A: $6{\cdot}10^{-4}$ in fast group and $8{\cdot}10^{-3}$ in thermal group, (ii) Test B: $8{\cdot}10^{-4}$ in fast group and $4{\cdot}10^{-3}$ in thermal group. Figures 7, 8, 13, and 14 demonstrate the relative difference between the scalar fluxes obtained by the splitting method and the HOFE method.

Figures 15-18 present the solutions of the D- and Q-problems for Test A obtained by the splitting and HOFE methods. Figures 19-22 demonstrate the same set of results for Test B. The figure for ϕ_D also show the solution of the modified diffusion. Smooth curves that represent the solution of the Q-problem calculated by the finite-volume method were obtained by means of a third-order polynomial interpolation function that fits coarse-cell edge values $\Phi_{Q,j}^{g,\pm}$ and two subcell-average values $\bar{\Phi}_{Q,j,i}^{g}$, i.e. the same polynomial function that is used to calculate necessary spatial moments of ϕ_Q for the fission source term in the D-problem.

These results show that the splitting method generates accurate solution for the D-problem. For the Q-problem, we used the second-order accurate finite-volume method and hence it is expected that there will be the difference compared to the results obtained by the HOFE method. In the fast group, the subcell average values and shapes of the Q-problem solutions generated by these two methods are fairly close to

each other. The difference increases in the thermal group. The overall effect on the resulting scalar flux is small, and the splitting method with the considered discretization produces sufficiently accurate scalar fluxes. We note that the splitting method uses the third-order polynomial to reconstruct the Q-problem solution, whereas the HOFE utilizes more accurate approximation based on the second-order polynomial combined with hyperbolic sine and cosine.

The relative difference in pin-cell average values compared to the fine-mesh results are listed in Tables IV and V, where we present the results of the proposed splitting method. Pins are numbered from left to right in each assembly. In Test A, the maximum absolute values of relative differences in fast group are $1{\cdot}10^{-3}$ and $6{\cdot}10^{-4}$ for MOX and UO_2 assemblies, respectively, and in thermal group are $9{\cdot}10^{-3}$ in MOX and $1{\cdot}10^{-2}$ in UO_2. In Test B, the maximum absolute values of relative differences in fast group are $2{\cdot}10^{-3}$ in MOX and $5{\cdot}10^{-4}$ in UO_2, and in thermal group $4{\cdot}10^{-3}$ and $7{\cdot}10^{-4}$, correspondingly. These results show that the splitting method reproduces the pin-cell average values of the scalar flux with high accuracy. Note that pin-power reconstruction using a form function will almost certanly produce even greater accuracy.

For the iteration process we used relative point-wise convergence criteria with values of 10^{-7} for the scalar flux and 10^{-8} for the eigenvalue. It took 15 and 16 iterations in case of the splitting method to calculate the solution of Test A and B, respectively. In case of the HOFE method the number of iterations are 13 and 17, correspondingly. Thus, the convergence behavior of the splitting method in these test problems is similar to that of the method without splitting.

Table IV. Test A. Relative difference in pin-cell average values for the splitting method

g	Region	pin #1	pin #2	pin #3	pin #4	pin # 5	pin # 6	pin #7	pin #8
1	MOX	$6{\cdot}10^{-4}$	$1{\cdot}10^{-3}$	$9{\cdot}10^{-4}$	$2{\cdot}10^{-4}$	$-7{\cdot}10^{-4}$	$-1{\cdot}10^{-3}$	$-1{\cdot}10^{-3}$	$3{\cdot}10^{-4}$
1	UO_2	$6{\cdot}10^{-4}$	$2{\cdot}10^{-4}$	$3{\cdot}10^{-4}$	$2{\cdot}10^{-4}$	$-9{\cdot}10^{-5}$	$-4{\cdot}10^{-4}$	$-5{\cdot}10^{-4}$	$-3{\cdot}10^{-4}$
2	MOX	$6{\cdot}10^{-3}$	$9{\cdot}10^{-3}$	$6{\cdot}10^{-3}$	$7{\cdot}10^{-4}$	$-4{\cdot}10^{-3}$	$-5{\cdot}10^{-3}$	$-5{\cdot}10^{-3}$	$-5{\cdot}10^{-3}$
2	UO_2	$1{\cdot}10^{-2}$	$4{\cdot}10^{-3}$	$-1{\cdot}10^{-3}$	$-3{\cdot}10^{-3}$	$-3{\cdot}10^{-3}$	$-3{\cdot}10^{-3}$	$-2{\cdot}10^{-3}$	$-1{\cdot}10^{-3}$

Table V. Test B. Relative difference in pin-cell average values for the splitting method

g	Region	pin #1	pin #2	pin #3	pin #4	pin # 5	pin # 6	pin #7	pin #8
1	MOX	$7{\cdot}10^{-4}$	$1{\cdot}10^{-3}$	$1{\cdot}10^{-3}$	$2{\cdot}10^{-4}$	$-1{\cdot}10^{-3}$	$-2{\cdot}10^{-3}$	$-1{\cdot}10^{-3}$	$5{\cdot}10^{-4}$
1	UO_2	$5{\cdot}10^{-4}$	$-1{\cdot}10^{-4}$	$3{\cdot}10^{-4}$	$4{\cdot}10^{-4}$	$7{\cdot}10^{-5}$	$-3{\cdot}10^{-4}$	$-5{\cdot}10^{-4}$	$-3{\cdot}10^{-4}$
2	MOX	$1{\cdot}10^{-3}$	$3{\cdot}10^{-3}$	$1{\cdot}10^{-3}$	$-2{\cdot}10^{-3}$	$-4{\cdot}10^{-3}$	$-4{\cdot}10^{-3}$	$-2{\cdot}10^{-3}$	$4{\cdot}10^{-3}$
2	UO_2	$7{\cdot}10^{-4}$	$6{\cdot}10^{-4}$	$-5{\cdot}10^{-4}$	$-7{\cdot}10^{-4}$	$-5{\cdot}10^{-4}$	$-2{\cdot}10^{-4}$	$1{\cdot}10^{-4}$	$6{\cdot}10^{-4}$

7. DISCUSSION

In this paper, we have developed a splitting method to solve the coarse-mesh discretized LOQD equations. The method effectively splits a problem into two parts. The D-problem captures a significant portion of the transport solution in the central part of assembly, and the Q-problem accounts for the complicated behavior of the transport solution in the vicinity of assembly boundaries. The calculation of discontinuity factors for the splitting method has been introduced, and corresponding interfacial conditions have been formulated for this particular method. Each part of the LOQD equations in the split form has been approximated by a

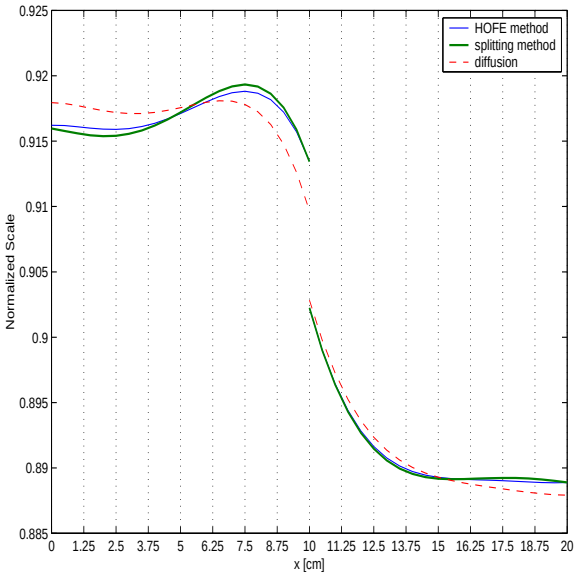

Figure 3. Test A. Fast scalar flux, $\phi^1(x)$.

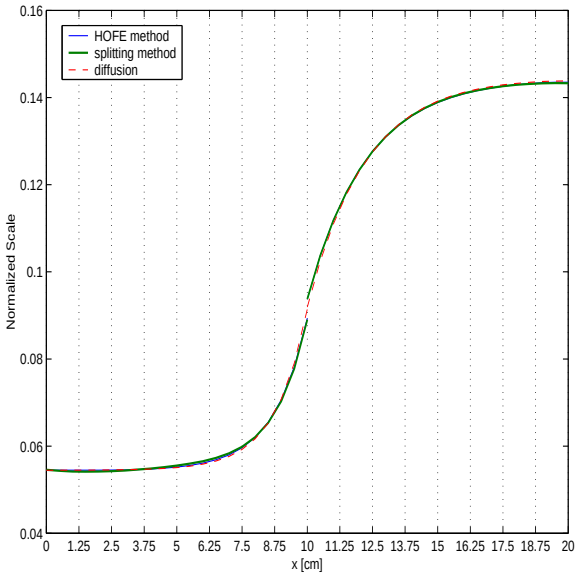

Figure 4. Test A. Thermal scalar flux, $\phi^2(x)$.

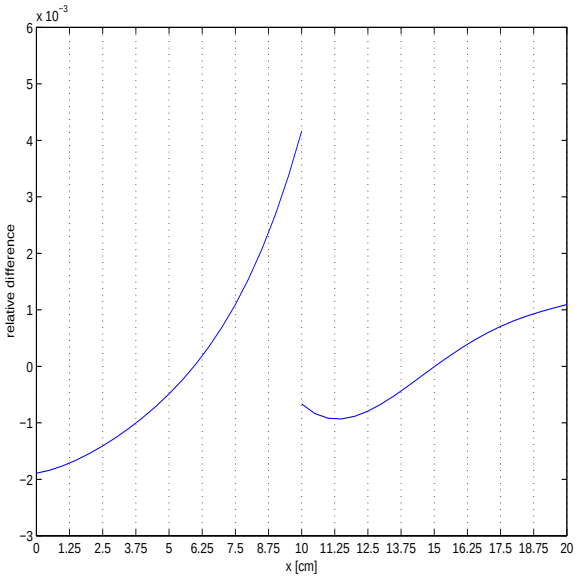

Figure 5. Test A. Relative difference in the fast scalar flux calculated by the diffusion equation compared to the coarse-mesh transport solution obtained from the LOQD equations.

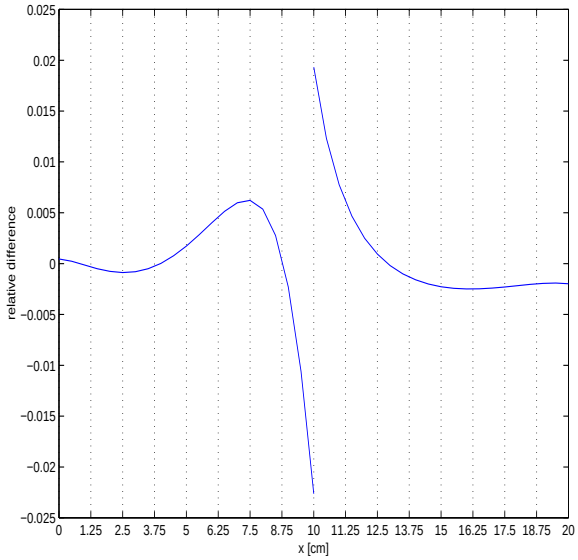

Figure 6. Test A. Relative difference in the thermal scalar flux calculated by the diffusion equation compared to the coarse-mesh transport solution obtained from the LOQD equations.

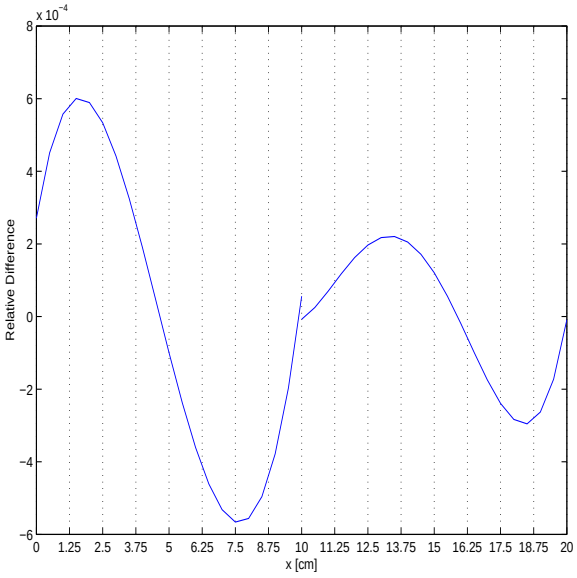

Figure 7. Test A. Relative difference in the fast scalar flux calculated by the splitting method compared to the results of the HOFE method.

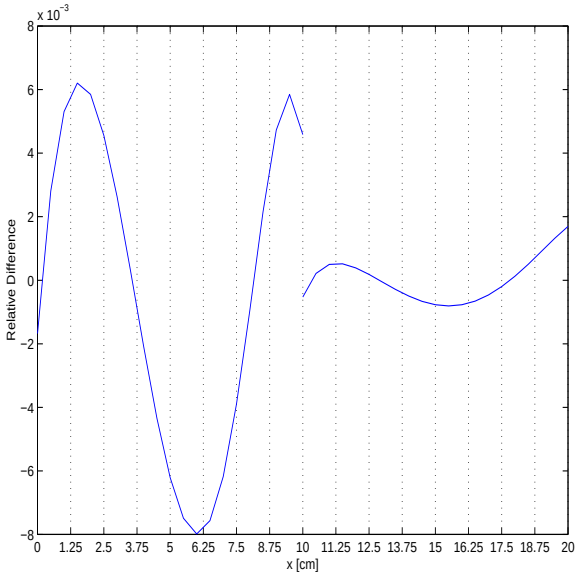

Figure 8. Test A. Relative difference in the thermal scalar flux calculated by the splitting method compared to the results of the HOFE method.

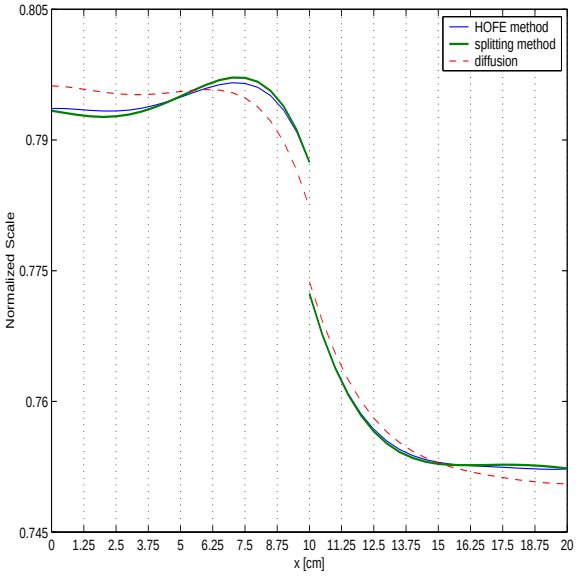

Figure 9. Test B. Fast scalar flux, $\phi^1(x)$.

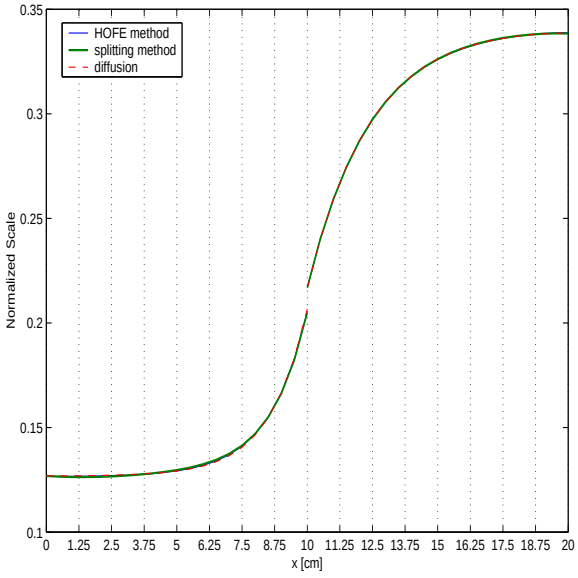

Figure 10. Test B. Thermal scalar flux, $\phi^2(x)$.

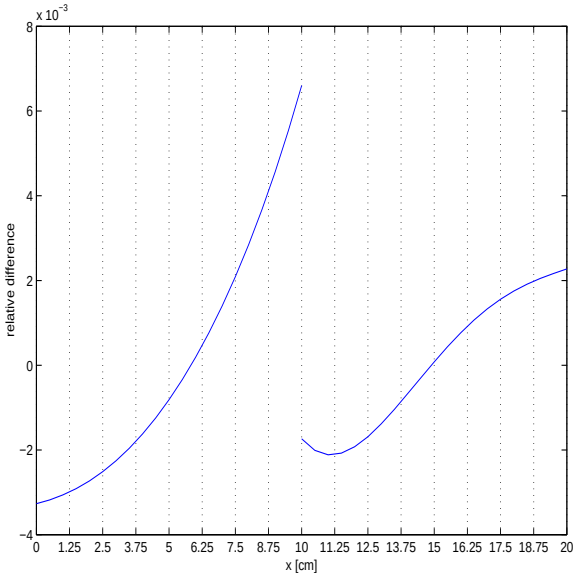

Figure 11. Test B. Relative difference in the fast scalar flux calculated by the diffusion equation compared to the coarse-mesh transport solution obtained from the LOQD equations.

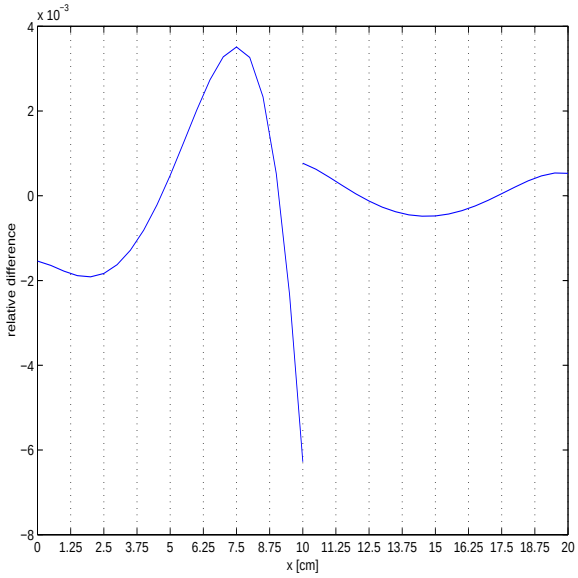

Figure 12. Test B. Relative difference in the thermal scalar flux calculated by the diffusion equation compared to the coarse-mesh transport solution obtained from the LOQD equations.

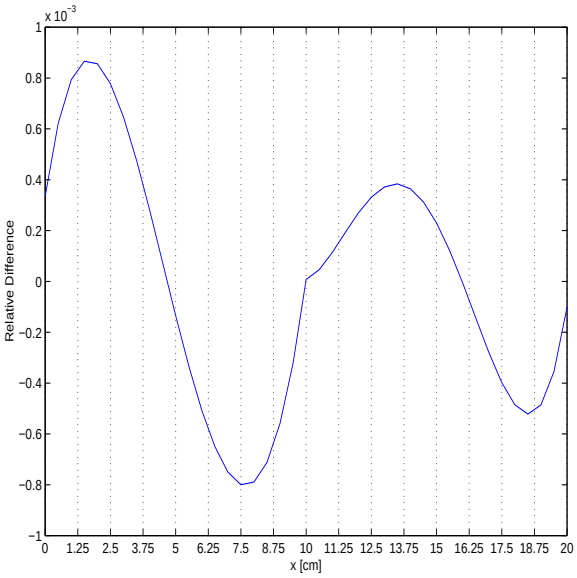

Figure 13. Test B. Relative difference in the fast scalar flux calculated by the splitting method compared to the results of the HOFE method.

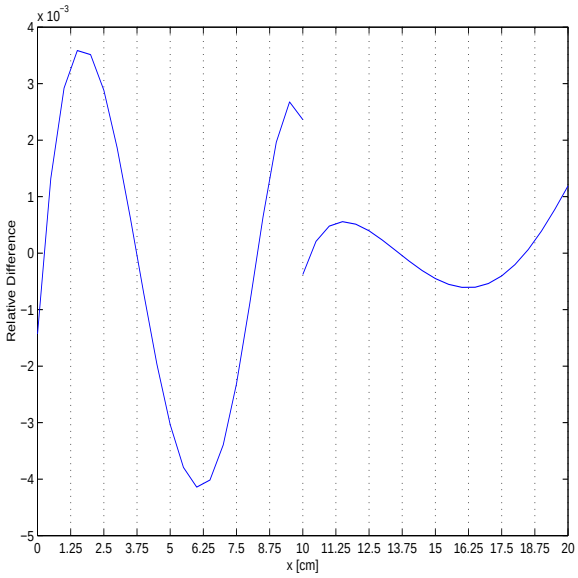

Figure 14. Test B. Relative difference in the thermal scalar flux calculated by the splitting method compared to the results of the HOFE method.

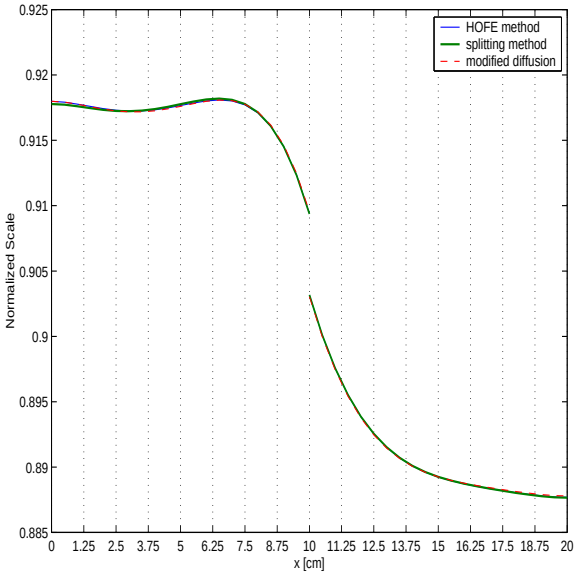

Figure 15. Test A. Solution of the D-problem in fast group, $\phi_D^1(x)$.

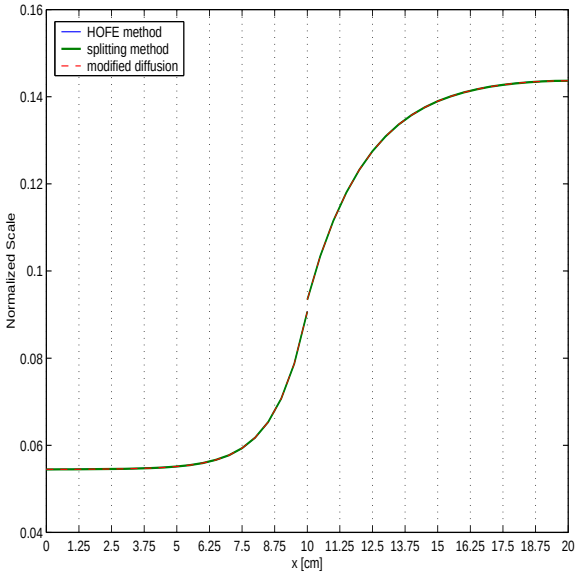

Figure 16. Test A. Solution of the D-problem in thermal group, $\phi_D^2(x)$.

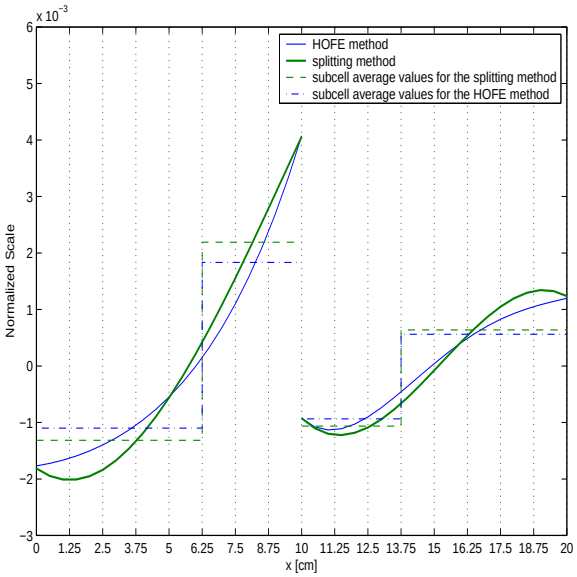

Figure 17. Test A. Solution of the Q-problem in fast group, $\phi_Q^1(x)$.

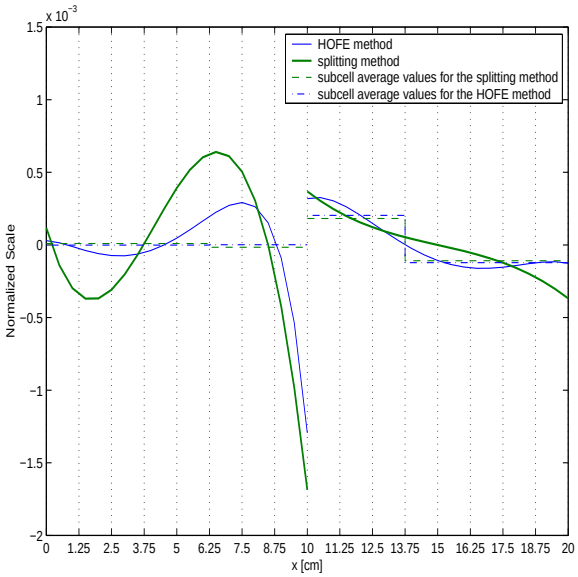

Figure 18. Test A. Solution of the Q-problem in thermal group, $\phi_Q^2(x)$.

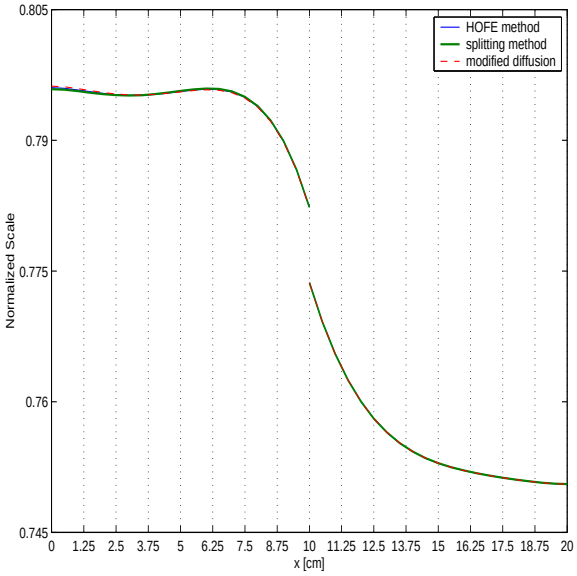

Figure 19. Test B. Solution of the D-problem in fast group, $\phi_D^1(x)$.

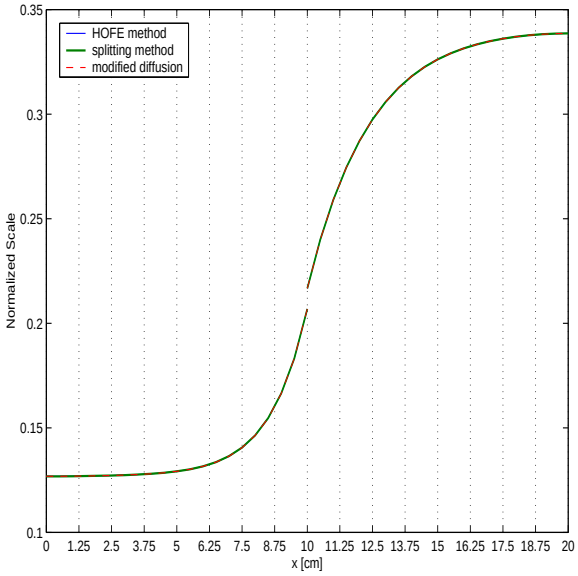

Figure 20. Test B. Solution of the D-problem in thermal group, $\phi_D^2(x)$.

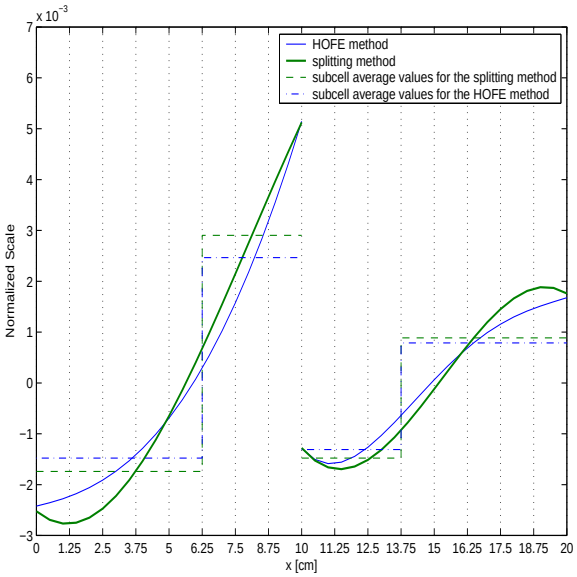

Figure 21. Test B. Solution of the Q-problem in fast group, $\phi_Q^1(x)$.

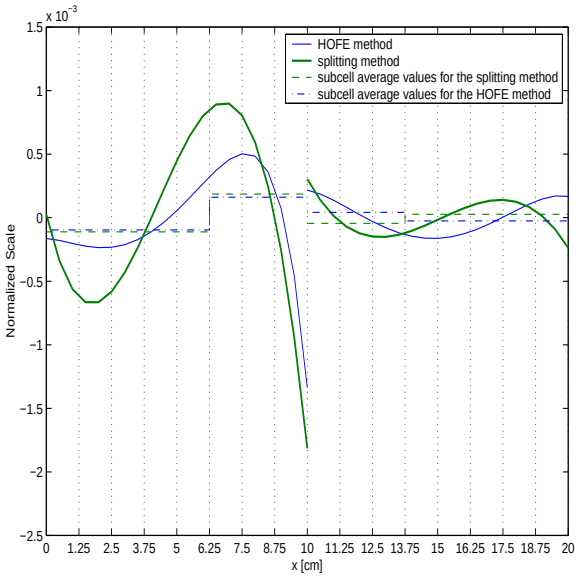

Figure 22. Test B. Solution of the Q-problem in thermal group, $\phi_Q^2(x)$.

different discretization scheme. The D-problem equations were approximated by means of the high-order finite element method. The Q-problem equations were discretized by using a finite volume method with second-order accuracy. Numerical results showed high accuracy of the proposed splitting method with the considered independent discretization of the equations of D- and Q- problems.

The successful performance of the splitting method in 1D geometry stimulates the efforts in extension of this method to multidimensional geometries. In 2D and 3D cases the solution of the LOQD equations discretized with high-order methods is rather computationally intensive problem. According to the proposed approach, one can split the LOQD problem into a D-problem that can be solved with current efficient methodologies for diffusion-type of equations and a Q-problem that can be discretized with a second-order finite-volume method because the solution of this problem is a small correction to solution of D-problem. Special interface conditions allow spatial decomposition of the Q-problem such that it can be solved in each coarse cell (part of assembly) independently of other cells. Thus, the presented splitting method enables us to reduce significantly computational costs for obtaining solution that very accurately accounts for transport effects in full-reactor calculations.

It is important to note that the proposed splitting method can be also utilized to upgrade current codes for full-reactor core calculations that are based on the diffusion theory. In such case, it is necessary to add solution of Q-problem and modify the definition of the diffusion coefficient as well as of the fission source term to account for the Q-problem solution. As a result, one gets a code based on transport theory calculations, provided that all extra group data and functionals are supplied from assembly-level calculations.

ACKNOWLEDGEMENTS

We would like to thank Todd Palmer and Kord Smith for helpful discussions. This work was supported by Nuclear Energy Initiative (NERI) Program of the US Department of Energy under grant No. DE-FG03-99SF21922.

REFERENCES

[1] K. S. Smith, “Assembly Homogenization Techniques for Light Water Reactor Analysis,” *Progress in Nuclear Energy*, **17**, pp. 303-335 (1986).

[2] V. Y. Gol’din, “A Quasi-Diffusion Method of Solving the Kinetic Equation,” *USSR Comp. Math. and Math. Phys.*, **4**, pp. 136-149 (1964).

[3] N. N. Aksenov and V. Y. Gol’din, “Computation of the Two-Dimensional Stationary Equation of Neutron Transfer by the Quasi-Diffusion Method,” *USSR Comp. Math. and Math. Phys.*, **19**, No. 5, 263-266 (1979).

[4] V. Y. Gol’din, “On Mathematical Modeling of Problems of Non-Equilibrium Transfer in Physical Systems,” in *Modern Problems of Mathematical Physics and Computational Mathematics*, Nauka, Moscow, 113-127 (1982) (in Russian).

[5] D. Y. Anistratov and M. L. Adams, “Consistent Coarse-Mesh Discretization of the Low-Order Equations of the Quasidiffusion Method,” *Trans. Am. Nucl. Soc.*, **83**, 250-251 (2000).

[6] K. T. Clarno and M. L. Adams, “Improved Boundary Conditions for Assembly-Level Transport Codes,” *Int. Conf. on the New Frontiers of Nuclear Technology: Reactor Physics, Safety and High-Performance Computing (PHYSOR 2002)*, Seoul, Korea, Oct. 7-10 (2002).

[7] R. Nes and T. S. Palmer, “An Advanced Nodal Discretization for the Quasi-Diffusion Low-Order Equations,” *Int. Conf. on the New Frontiers of Nuclear Technology: Reactor Physics, Safety and High-Performance Computing (PHYSOR 2002)*, Seoul, Korea, Oct. 7-10 (2002).

[8] D. Y. Anistratov, “Homogenization Methodology for the Low-Order Equations of the Quasidiffusion Method,” *Int. Conf. on the New Frontiers of Nuclear Technology: Reactor Physics, Safety and High-Performance Computing (PHYSOR 2002)*, Seoul, Korea, Oct. 7-10 (2002).

[9] V. Y. Gol’din and A. V. Kolpakov, “Nonlinear Marching Method for Solving the Multidimensional Diffusion Equation,” *Preprint of the Keldysh Institute for Applied Mathematics*, the USSR Academy of Sciences, No. 22 (1982) (in Russian).

[10] V. Y. Gol’din, D. A. Gol’dina and A. V. Kolpakov, “The Solution of Two-Dimensional Stationary Quasidiffusion Problem,” *Preprint of the Keldysh Institute for Applied Mathematics*, the USSR Academy of Sciences, No. 49 (1982) (in Russian).

[11] E. N. Aristova and A. V. Kolpakov, “A Combined Finite Difference Scheme for an Elliptic Operator in an Oblique-Angled Cell,” *Mathematical Modeling and Computational Experiment*, **1**, 187-196 (1993).

[12] E. N. Aristova, V. Y. Gol’din, and A. V. Kolpakov, “Multidimensional Calculations of Radiation Transport by Nonlinear Quasi-Diffusion Method,” *Proceeding of ANS International Conference on Mathematics and Computation, Reactor Physics and Environmental Analysis in Nuclear Applications*, Sept. 27-30, 1999, Madrid, Spain, 667-676 (1999).

[13] K. T. Clarno and M. L. Adams, *this proceedings*.

[14] D. Y. Anistratov, “Consistent Spatial Discretization of the Low-Order Quasidiffusion Equations on Coarse Grids,” this proceedings (2003).

[15] D. Y. Anistratov and V. Y. Gol’din, “Nonlinear Methods for Solving Particle Transport Problems,” *Transport Theory and Statistical Physics*, **22**, No. 2&3, 42-77 (1993).

[16] K. S. Smith, *private communication*.